Journal of Water Resource and Protection, 2019, 11, 789-809
http://www.scirp.org/journal/jwarp
ISSN Online: 1945-3108
ISSN Print: 1945-3094

Removing Iron Ions Contaminants from Groundwater Using Modified Nano-Hydroxyapatite by Nano Manganese Oxide

Mohammed Abd-El-Aal Ahmed Ayash[1]*, Tarek Ahmed Seaf Elnasr[2,3], Madiha Hassan Soliman[4]

[1]Sohag Company for Water and Waste Water, Dar El Salam, Sohag, Egypt
[2]Chemistry Department, Faculty of Science, Al-Azhar University, Assiut, Egypt
[3]Chemistry Department, Collage of Science, Jouf University, KSA
[4]Chemistry Department, Faculty of Science, Helwan University, Cairo, Egypt
Email: *chemistayash@gmail.com, tarekseaf@gmail.com, drmadihahasan@yahoo.com

How to cite this paper: Abd-El-Aal Ahmed Ayash, M., Elnasr, T.A.S. and Soliman, M.H. (2019) Removing Iron Ions Contaminants from Groundwater Using Modified Nano-Hydroxyapatite by Nano Manganese Oxide. *Journal of Water Resource and Protection*, **11**, 789-809.
https://doi.org/10.4236/jwarp.2019.116048

Received: May 26, 2019
Accepted: June 27, 2019
Published: June 30, 2019

Abstract

In this article, we study modified nano-hydroxyapatite (HAp) by nano manganese oxide (Mn_3O_4) as adsorbent material to remove iron ions from groundwater. Different parameters were studied to option optimum conditions of removing such as contact time, pH, initial concentration, a dosage of adsorbent, agitation speed and temperature. Kinetics studies included first order (R^2 = 0.915), pseudo-first order (R^2 = 0.936), second order (R^2 = 0.948), pseudo-second order (R^2 = 0.995), Elovich equation model (R^2 = 0.977), intraparticle diffusion (R^2 = 0.946), Natarajan and Khalaf (R^2 = 0.915) were carried out, the obtained results revealed that the pseudo-second order is the best to describe the adsorption process because the correlation coefficient is approaching one (R^2 = 0.995). Adsorption isotherm was calculated by using Freundlich, Langmuir and Temkin constants, adsorption capacity from Langmuir model was 0.606 mg/g. Thermodynamic parameters (ΔG, $\Delta H = -51$ KJ/mol, and $\Delta S = -142$ (KJ/mol)) for the adsorption process were also calculated and discussed.

Keywords

Groundwater, Adsorption, Nano Materials, Hydroxyapatite, Manganese Oxide, Iron Ions, Kinetic, Thermodynamic

1. Introduction

Groundwater is an important resource for the livelihoods and food security of billions of people. It is one of the most difficult problems that pollute the groundwater and the presence of iron. Therefore, in this article, we try to find a solution to the problems of iron in the groundwater [1] [2].

Among the appropriate solutions to remove or reduce the proportion of iron in the groundwater is Ion exchange [3], Reverse osmosis [4], Chemical precipitation [5], Electrolysis [6] and Adsorption [7], the choice of which depends upon the type and concentration of both sorptive material and sorbent employed, as well as their costs [8].

Among these, the adsorption method is more commonly used, adsorption is an effective technology to remove different contaminated from aqueous solutions. In this process, a very high rate of adsorption and excretion occurs. The simple function has caused this method to be one of the best ways to remove iron ions from groundwater such as Polyvinyl alcohol was used for removal of bromothymol blue and methylene blue from [9]. Removal of natural organic matter and its constituents from water by metal oxides and hydroxides based adsorbents were investigated [10]. Fluoride removal capacity from drinking water by Adsorption using nano-sized Alumina and Zirconia modified Alumina was tested [11]. Removal of Cu(II) and Zn(II) by unmodified Lignocellulosic Fibrous Layer of Palm Tree Trunk-Single was studied [12]. Removal of Cu(II) ions from water by rice husk (S.E. Abd Elhafez *et al.* 2016) [13], Pb (II), La (III), and Ag (I) ions was removed from aqueous solutions using mediated cellulose nanofibers [14]. Adsorptive of ibuprofen and diclofenac from water using metal-organic framework-derived porous carbon was investigated [15]. Removal of Cr(VI) by a free metal material containing only C, N and O, and having environmental friendliness, was studied [16]. Removal of benzotriazole and benzimidazole from water over a Co-based metal azolate framework MAF-5(Co) was investigated [17].

In this work, we have used modified nano hydroxyapatite by (Mn_3O_4) nanoparticles to remove the iron ions from water by adsorption; parameters such as contact time, pH, adsorbent dosage, stirring speed and temperature were investigated. Kinetic, Isotherm Adsorption and Thermodynamic parameters (ΔG, ΔH, and ΔS) for adsorption process were also calculated and discussed.

2. Materials and Methods

2.1. Apparatus

We had all the measurements of pH using Misura Line 1010 pH meter (Romania). All samples are stirred and heated by multiple Heating Magnetic Stirrer (VELP Scientifica) during experimental procedures as well, as micropipette (100 - 1000 μL) is also used. Spectrophotometer Instruments (CECIL3021), Brand (Cambridge, England). Determine the iron ions by Phenanthroline method. The samples were first mixed with KBr and then pressed into pellets. X-ray powder diffraction (XRD) data were collected at room temperature using a Philips 1710 Diffractometer. The patterns were run with Cu target and Ni filter (λ = 1.5418

A˚) at 40 KV and 30 mA in the range of 2θ, with a scanning speed of 06 deg/s. Fourier transform infrared spectroscopy (FTIR) data were collected using a Perkin-Elmer spectrometer model 1430 in the wave number range from 4000 to 400 cm^{-1} Examination on the TEM: Samples were examined by carbon coated grids with a JEOL 1010 Transmission Electron Microscope, made in Japan, at the Regional Center for Mycology and Biotechnology (RCMB), Al-Azhar University.

2.2. Procedures

2.2.1. Synthesis of Hydroxyapatite (HAp)

We have prepared HAp powder using the titration between both H_3PO_4, adwic 85% in burette and $CaCl_2{\cdot}2H_2O$, Sigma-Aldrich, 99% - 103% in a beaker until adjustment the pH at a value of 10. Through the addition of NH_4OH solution (adwic 30%) during the mixing process using a hotplate for heating the reaction mixture and stirring according to the following equation:

$$\mathbf{10CaCl_2{\cdot}2H_2O+6H_3PO_4 + 20NH_4OH \rightarrow Ca_{10}(PO_4)_6(OH)_2 + 20NH_4Cl + 38H_2O \ (I)}$$

The mixture was heated in a microwave oven for 10 min until completely dryness and formation the precipitate, and then it was washed with distilled water and filtrated. The precipitate dried by microwave for 4 min [18].

2.2.2. Synthesis of Manganese Oxide

We can manufacture nano-manganese oxide (Mn_3O_4) by oxidation of $MnCl_2$ solution with a concentrated H_2O_2 solution, followed by the addition of an NH_3 aq. solution. The suspension thus obtained was treated at 90˚C [19]. With microwave for 7 mint to dryness and formation the precipitate, then it was washed with distilled water and filtrated. The precipitate dried by microwave for 3 min.

2.2.3. Synthesis of Modified Hydroxyapatite Manganese Hydroxide (HApMn)

We have been able to prepare three modifications to test the removal of iron ions first (0.04 HAp:0.06 Mn_3O_4) second (0.06 HAp:0.04 Mn_3O_4) and the third (0.08 HAp:0.02 Mn_3O_4). The percentage of removing iron ions were (R%) = 49%, 47%, and 30% respectively. We chose (0.06 HAp:0.04 Mn_3O_4) R% = 47% and have found that the best modification is. Three composed of Modification of HAp by Mn_3O_4 were prepared and exam to remove iron ions, to complete this study.

2.3. Analytical Methods

Amount of adsorbent of iron on happening at any time (q_t) was calculated as follows [8] [9]:

$$q_t = (C_o - C_t)V/m \quad (1)$$

where, C_o and C_t are the concentrations of iron ions at initial and equilibrium time, respectively (mg/L), V is the solution volume (L) and m is the mass of dry adsorbent used (g). At equilibrium, $q_e = q_t$ and $C_t = C_e$; therefore, the amount of sorbed metal ion (q_e) was calculated according to Equation (2)

$$q_e = (C_o - C_e)V/m \tag{2}$$

The removal efficiency (RE%) is calculated according to the following equation [12]:

$$\text{RE}(\%) = \left((C_o - C_e)/C_o\right) \times 100 \tag{3}$$

3. Results and Discussion

3.1. Characterizations

Figure 1(a) shows the FTIR (Fourier transform infrared spectroscopy) of HAp. The broad bands in the regions 1600 - 1700 cm^{-1} and 3200 - 3600 cm^{-1} correspond to H-O-H bands of lattice water. The bands characteristics of the phosphate and hydrogen phosphate groups in apatite environment are observed at 565, 632, 603, 962, and 1000 - 1100 cm^{-1} for PO_4^{3-} and at 875 cm^{-1} for HPO_4^{2-} [18].

FTIR of the Manganese Oxide sample is shown in Figure 1(b). Several absorption bands can be observed at 500 - 1000 cm^{-1} for (Mn-O), 3000 - 3500 cm^{-1} stretching, the 1636. While the 606, 564, 510.2 and 417 cm^{-1} bands should be ascribed to the Mn–O vibrations in MnO_6 octahedral [19].

FTIR results indicate the presence of some bounded water to HApMn.

Figure 2(a) and Figure 2(b) shows XRD (X-ray Diffraction) patterns of the

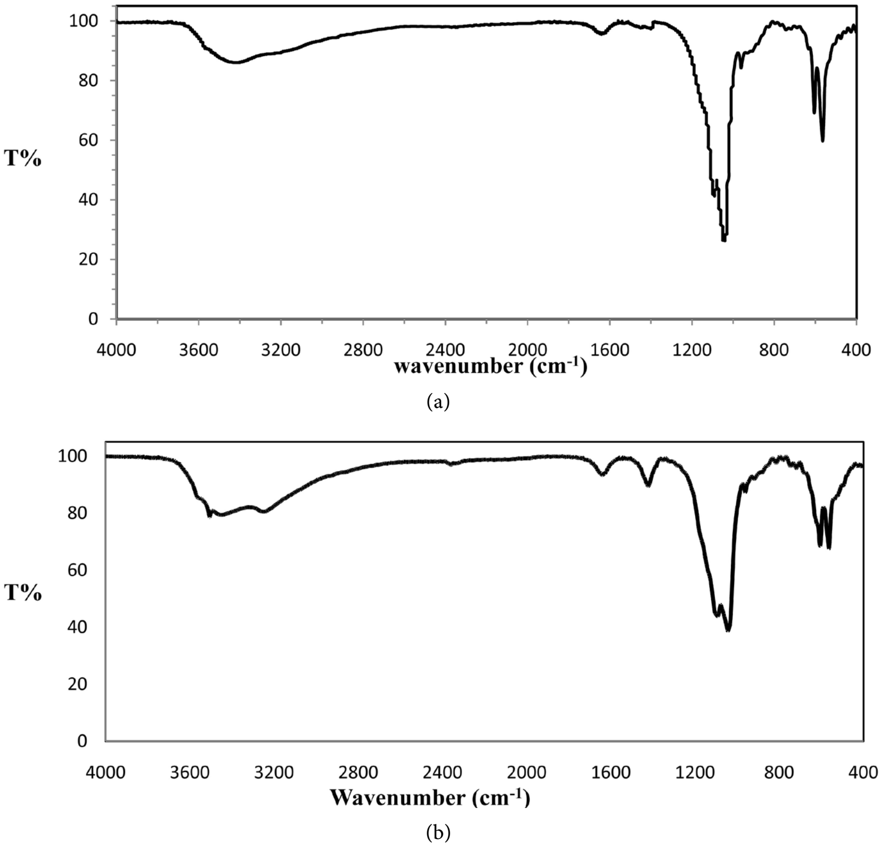

(a)

(b)

Figure 1. FTIR spectra for (a) HAp and (b) HApMn.

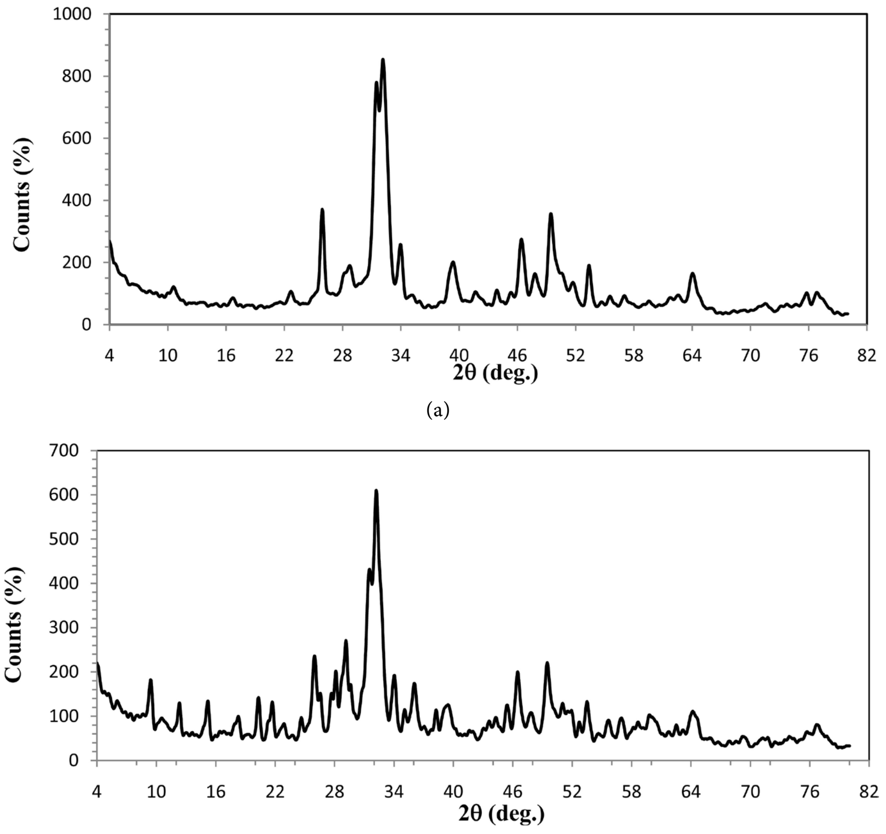

(a)

(b)

Figure 2. (a) XRD profiles for prepared HAp; (b) XRD profiles for Mn_3O_4.

HAp and Mn_3O_4 samples, respectively. The intensive diffraction peaks appeared at 25.9, 28.9, 31, 32.3, 33, 33.9, 36.9, 39.2, 44.3, 46.4, 47.8, 49.5, 51.22, 53.4, 58.4, 60.2, 64.5, 74.4, 76.7 and 55.9 are assigned to the characteristic peaks for Mn-O, and the peaks occurred at respectively, should be ascribed to the characteristic peaks for Mn-O [19]. Hence, the sample appears to be composed of a majority of HApMn. Scherer equation can be written as [7] [20]:

$$D = K\lambda/\beta\cos\theta \tag{4}$$

where D is the crystal size (nm), λ is the wavelength of X-ray light, β is the full width of the half maximum of the diffraction peak, and θ is the diffraction angle. Shape factor of K is usually taken as 0.9. It was found that the particle sizes were 4.2 nm and 3.6 nm for HAp and Mn_3O_4, respectively. The result is tabulated in Table 1.

Figure 3(a) and Figure 3(b) show TEM (Transmission electron microscopy) of HAp profiles and Mn_3O_4 profiles respectively.

3.2. Study of Adsorption Factors

We have used a Patch method for all adsorption work, 100 ml of sample (2- 10) ppm, temperature (25 - 75)˚C, pH (3 - 8), contact time (5 - 90) min, the speed of agitation (100 - 8000) rpm, iron ions concentration was measured before placing

Table 1. Size of HAp and Mn_3O_4 calculate by XRD (Scherer equation) and measured by TEM.

Calculate by Scherer equation (XRD)		From TEM		
HAp	Mn_3O_4		HAp	Mn_3O_4
Distance	Distance	Statistical Function	Distance	Distance
nm	Nm	Base Unit	nm	Nm
22.62	8.91	Count	5	5
26.38	9.09	Mean	23.58	9.20
18.66	11.52	Minimum	18.66	8.14
28.42	8.34	Maximum	28.42	11.52
21.79	8.14	Standard Deviation	3.86	1.35
		Cal. by XRD	4.2	3.6

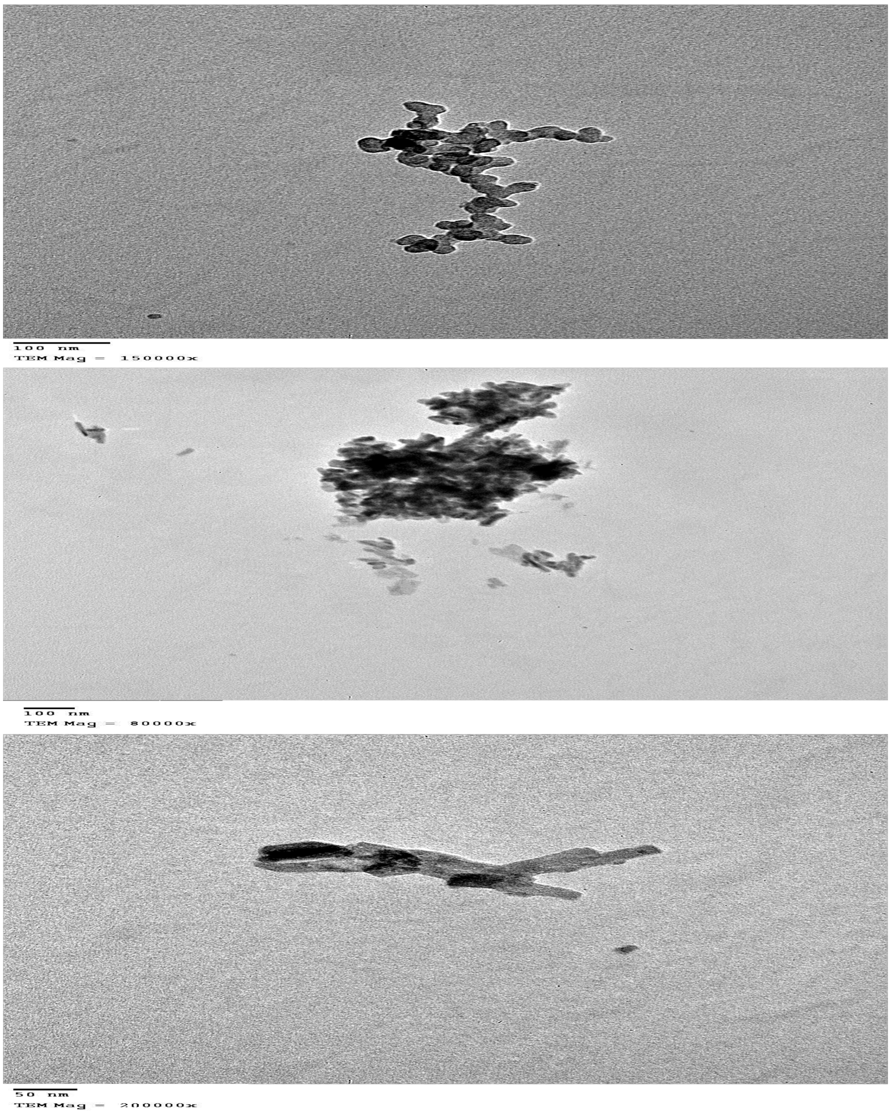

(a)

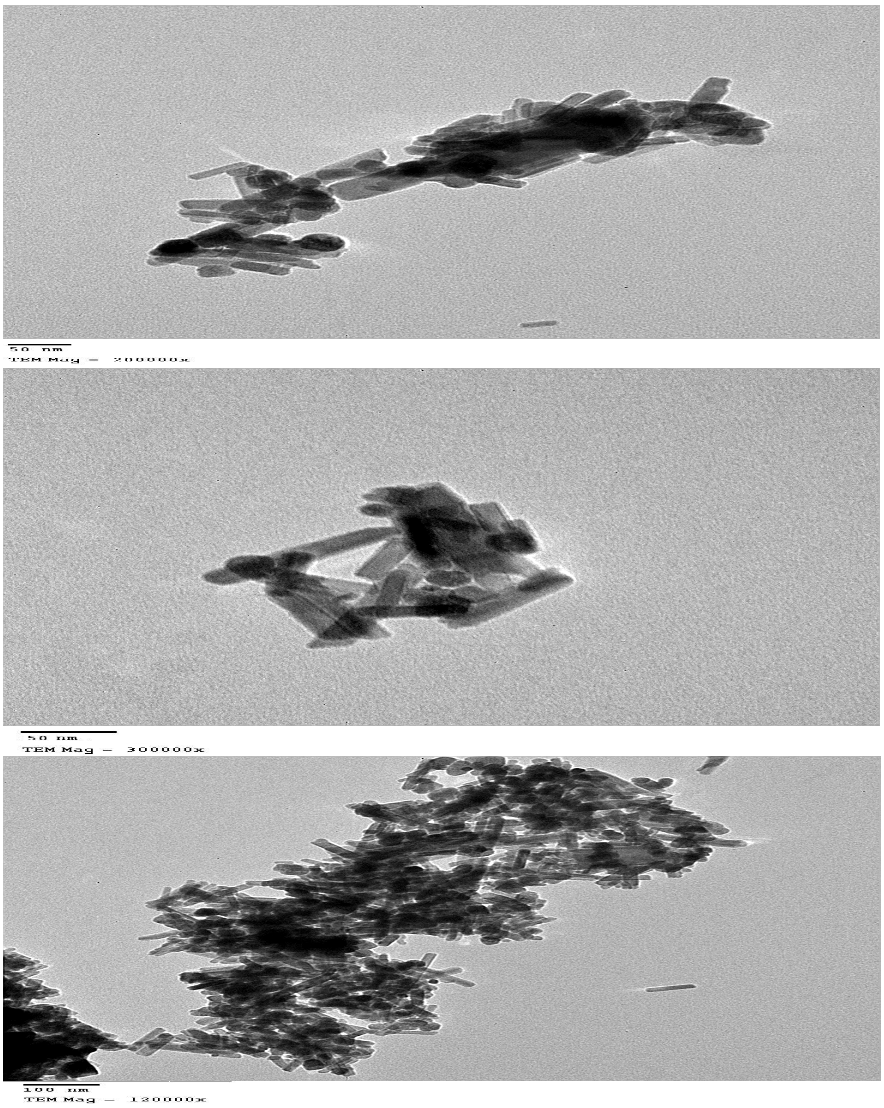

(b)

Figure 3. (a) TEM profiles for prepared of HAp; (b) TEM profiles for prepared Mn_3O_4.

the adsorbent and after putting them for different samples obtained from different wells as shown in **Table 2**. Various adsorption parameters for the effective removal of iron ions using modified hydroxyapatite as an adsorbent from aqueous solution were studied and optimized.

3.2.1. Effect of Contact Time

We have studied the effect of contact time in different time periods ranging from 5 to 90 min with the initial metal concentration of 2 ppm iron ions in presence 0.1 g of HApMn with continuous stirring at 400 rpm and at pH 6 [21]. Remove iron ions over time, where it was about 25% in 5 minutes and reached 60% in 90 minutes see **Figure 4**.

3.2.2. Effect of pH

PH is an important factor in the adsorption process. The pH of 3 - 8 is determined

Table 2. Iron ion concentrations of well samples before and after treatment.

no	Place (well name)	well name	Before Ppm	After Ppm
1	New Awolad Khalf	3	0.94	0.22
2	New Awolad Khalf	4	1.03	0.23
3	New Awolad Khalf	5	1.1	0.24
4	Arab Elataiat south	2	0.68	0.155
5	Old Elkhamima	3	0.58	0.12

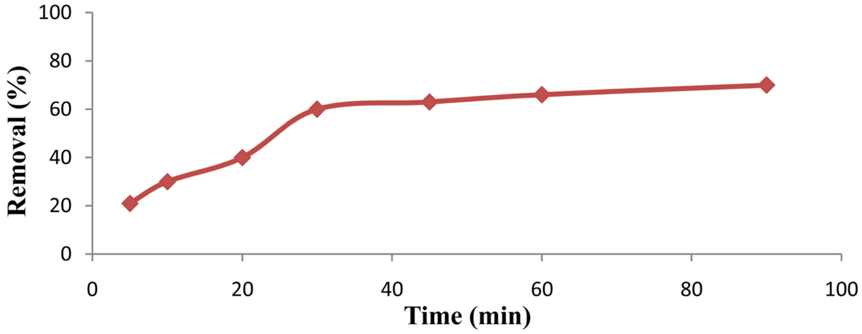

Figure 4. Effect of contact time on iron ions removal using HApMn.

by using 30% ammonia solution or 37% hydrochloric acid solution and the same conditions as above. Note that the increase in pH increases the removal iron ions (see **Figure 5**). It may be due to precipitation of iron ions as Fe^{+3} hydroxide brown precipitate [22].

3.2.3. Effect of Agitation Speed

The effect of the stirring speed on the removal of iron ions under the same experimental conditions is studied by agitation Speed (100 - 800) rpm. The efficiency of the removal was found to increase with increased agitation speed (see **Figure 6**). Iron ions increase the speed of stirring [23].

3.2.4. Effect of Initial Concentration of Iron Ions

By studying the effect of iron ion concentration per 100 ml, we found that the removal efficiency was reduced by increasing the concentration of iron per 100 ml see **Figure 7** [24].

3.2.5. Effect of Temperature

Under the same experimental conditions the effect of temperature on iron ions removal was studied by varying the temperature from 25˚C to 75˚C. As we see from **Figure 8**, as the temperature increases the removal percentage increase [25].

3.2.6. Applications of the Method

Around 100 ml of sample (well water) at pH about 7.4, the temperature at 30˚C, stirring at 400 rpm, stirring time 30 min was used to measure iron ions concentrations.

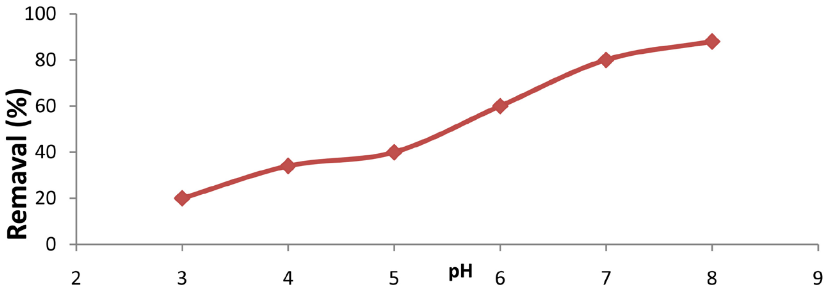

Figure 5. Effect of pH on iron ions removal using HApMn.

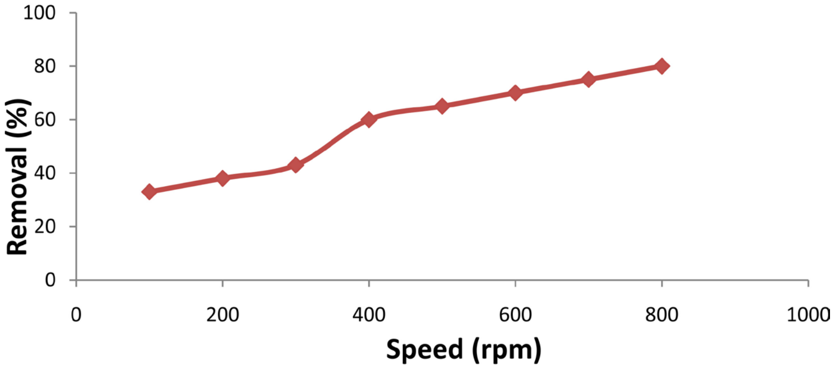

Figure 6. Effect of agitation speed on iron ions removal using HApMn.

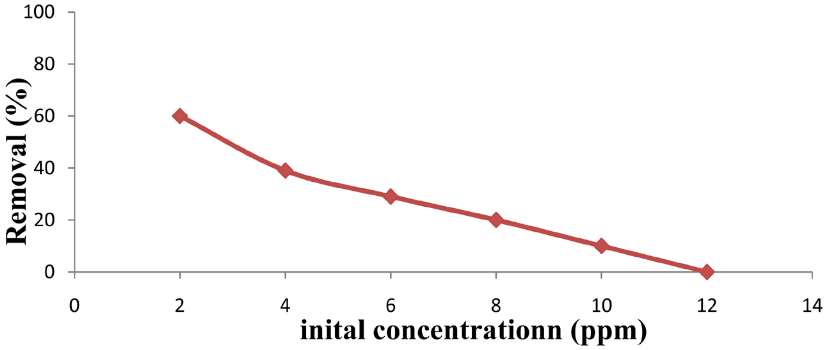

Figure 7. Effect of initial concentration on iron ions removal using HApMn.

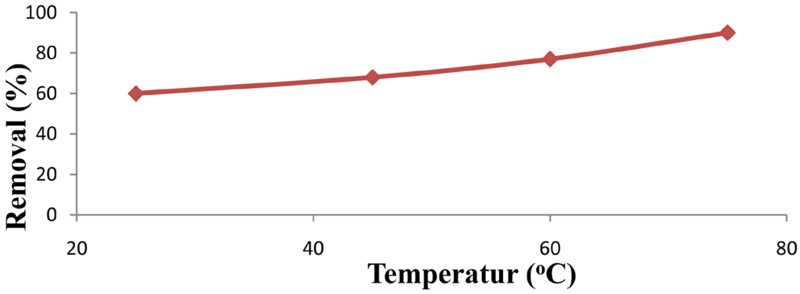

Figure 8. Effect of temperature on iron ions removal using HApMn.

3.3. Kinetics Modeling

We have done a study the kinetic of adsorption and adsorption rate controls; we found a metal ion uptake rate with a residence time of adsorbate uptake at solid interface solution. We have studied seven equations models, the first-order rate equation, pseudo-first order rate equation, second-order rate equation, pseudo-second order rate equation, intra-particle diffusion, and Elovich equations. See Table 3 for the parameter values.

3.3.1. First Order Kinetic Equation

The equation of a straight line is applicable [12] [26]:

$$-\ln\left(C_t/C_o\right) = K_1 t \tag{5}$$

where, C_t (mg/L) is the concentration at a given time t and C_o (mg/L) is initial concentration of iron ions in solution. K_1 (min^{-1}) is the first order rate constant. The regression R^2 obtained by the linear plot of $-\ln(C_t/C_o)$ against t (Figure 9), is shown in Table 3, R^2 was greater than 0.9, which indicates a good fit to the experimental data.

3.3.2. Second Order Kinetic Equation

The linear version is given by this relationship [12] [26]:

$$\left(1/C_t\right) - \left(1/C_o\right) = K_2 t\,. \tag{6}$$

where, k_2 [L/mg/min] is the second order rate constant for the adsorption process, determined from the linear plot of $(1/C_t - 1/C_o)$ against t, shown in (Figure 10) for iron ions. See Table 3, for the value of the constants. The

Table 3. Summary of kinetic modeling parameters.

No	Kinetics model	Parameters	Value
1	First-order rate equation $-\ln(C_t/C_o) = K_1 t$	**K_1 (min^{-1})**	0.0116
		R^2	0.915
2	Second order rate equation $[1/C_t] - [1/C_o] = K_2 t$	**K_2 (L/mg·min)**	0.013
		R^2	0.948
3	Lagergren pseudo first-order equation. $\mathrm{Ln}\,(q_e - q_t) = \ln q_e - K_1 t$	**K_1 (min^{-1})**	−0.018
		R^2	0.936
4	Pseudo second-order rate equation $t/q_t = 1/K_2 q_e^2 + t/q_e$	**K_2 (g/mg·min)**	0.036
		q_e	1.677
		R^2	0.995
5	Intraparticle diffusion $q_t = K_p t^{1/2} + c$	**c (mg/g)**	0.196
		R^2	0.946
		K_p (mg/g·min$^{1/2}$)	0.143
6	Elovich equation model $q_t = [1/\beta]\ln[\alpha\beta] + [1/\beta]\ln t$	**R^2**	0.977
		α	0.214
		β (g/mg)	2.691
7	Natarajan and Khalaf $\mathrm{Ln}(C_o/C_t) = Kt$	**K (min^{-1})**	0.0116
		R^2	0.915

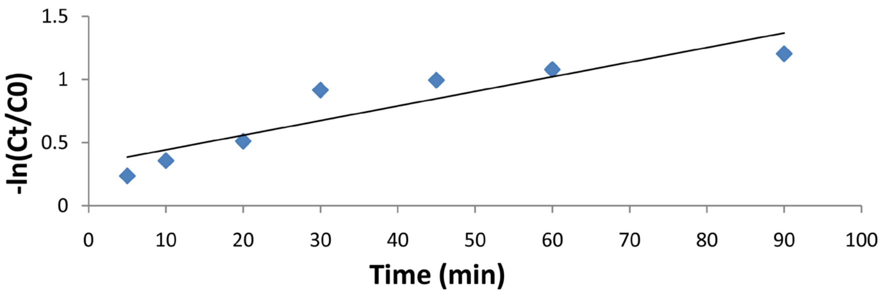

Figure 9. First Order Kinetic Equation plot for the adsorption of iron ions on HApMn.

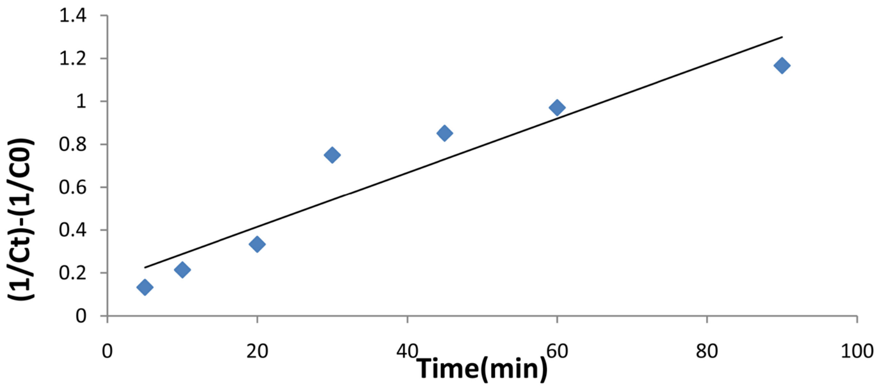

Figure 10. Second order rate equation plot for the adsorption of iron ions on HApMn.

regression value (R^2) is greater than 0.9 for iron ions. Indicating that the equation can be applied to experimental data for iron ions.

3.3.3. Pseudo First Order Kinetic Equation

The mathematical relationship to describe the pseudo-motif model proposed by Lagergren is shown in equation [12] [27]:

$$\ln\left(q_e - q_t\right) = \ln q_e - K_1 p_t \tag{7}$$

where K_1 is the rate constant of pseudo-first order adsorption (L/min). q_e and q_t are adsorption capacity (mg/g) at equilibrium and at any time t, respectively. The value of the constants q_e, k_1 and R^2 obtained from the linear plot of $\ln(q_e - q_t)$ vs t (**Figure 11**) are shown in **Table 3**. The regression rate $R^2 > 0.9$ For iron ions.

3.3.4. Pseudo-Second Order Kinetic Equation

The linear relationship of pseudo-second order kinetic model is given by [12] [23] [24] [25] [27] [28]:

$$t/q_t = 1/K_2 q_e^2 + t/q_e \tag{8}$$

where K_2 (g/mg/min) is the rate constant of pseudo-second order adsorption rate constant. The values of k_2, R^2 and q_e were calculated from the plots of t/q_t on the vertical axis, and t (min) on the horizontal axis (**Figure 12**) as shown in **Table 3**. The regression $R^2 > 0.9$, for iron meaning that this model provided the best fit for the adsorption data.

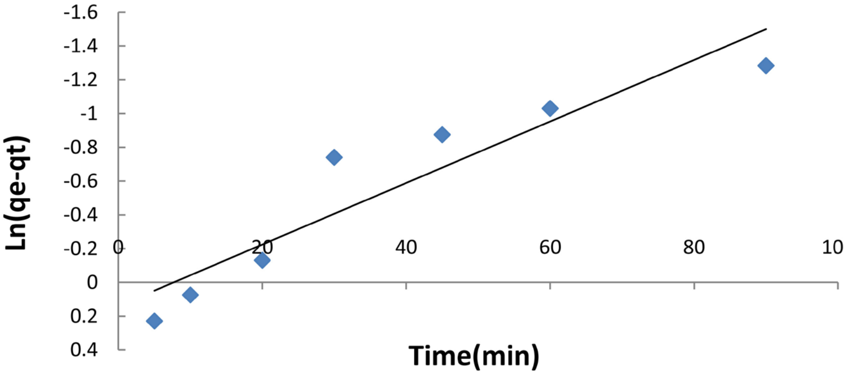

Figure 11. Pseudo first-order kinetic plot for the adsorption of iron ions on HApMn.

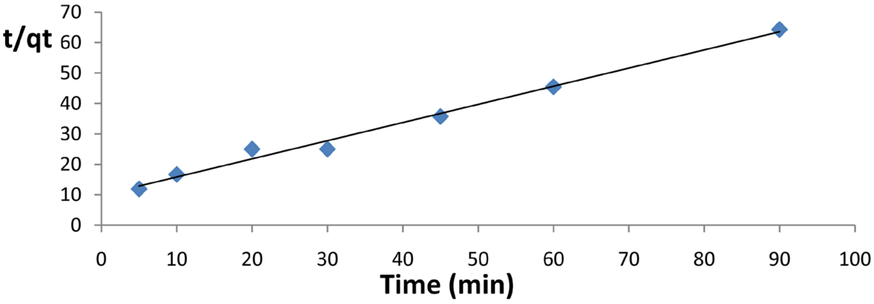

Figure 12. Pseudo second order rate plot for the adsorption of iron ions on HApMn.

3.3.5. Elovich Equation

The Elovich equation used to describe the kinetics of chemisorption of gas on solids, The linear relationship is given by [12] [23] [24] [25] [27] [28]:

$$q_t = (1/\beta)\ln(\alpha\beta) + (1/\beta)\ln t \tag{9}$$

where, the constants α and β were obtained from the slope and intercept of the linear plot of q_t (mg/g) against ln(t, min) as shown in (Figure 13), for the adsorption of iron ions on HApMn.

3.3.6. Intra-Particle Diffusion Rate Equation

The intra-particle diffusion equation [12] [28] [29] [30] is given as Equation (10) shown in Figure 14.

$$q_t = kp_t^{1/2} + C \tag{10}$$

where, K_p (mg/g·min$^{1/2}$) is the intraparticle diffusion rate constant and C is the intercept. by drawing q_t on the Y-axis against t (min) on X-axis we can find the slope, intercept and correlation coefficient as seen in Table 3, it was observed that the intraparticle diffusion rate constant increased with an increase in initial concentrations.

3.3.7. Natarajan and Khalaf

Natarajan and Khalaf equation [31] developed a relationship between the initial concentration and concentration at any time. The linear form is expressed as:

$$\ln(C_o/C_t) = K_n \cdot t \tag{11}$$

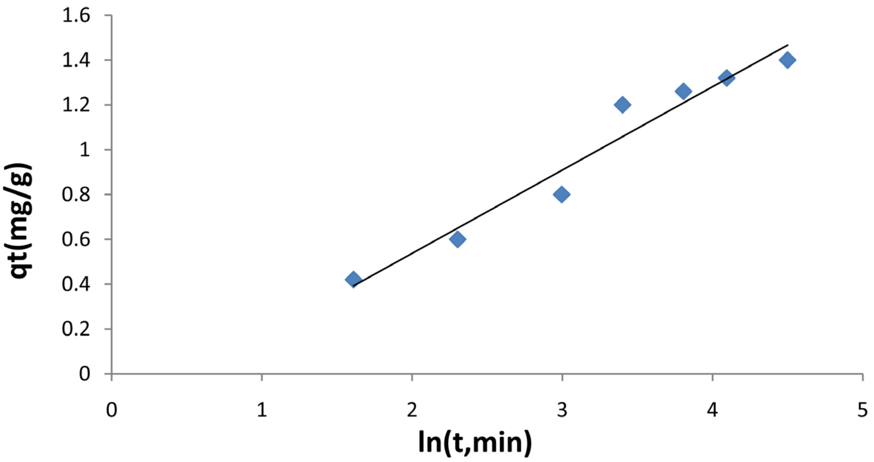

Figure 13. Elovich plot for the adsorption of iron ions on HApMn.

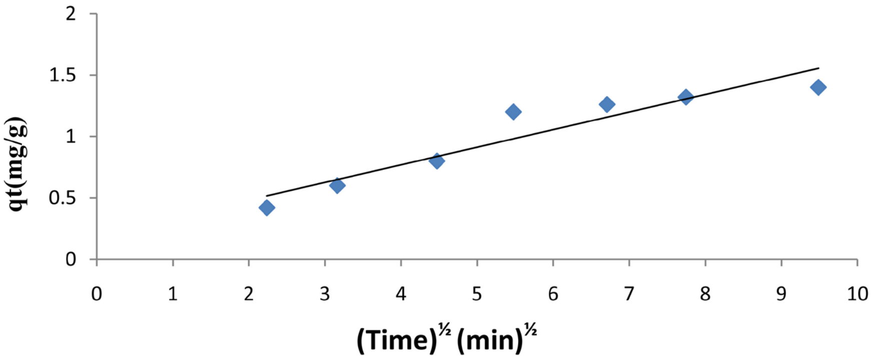

Figure 14. Intraparticle diffusion equation plot for the adsorption of iron ions on HApMn.

where, C_t is the concentration of iron (mg/L) at time t. The plot of $\ln(C_o/C_t)$ against t will give a straight line and the value of k_n can be obtained from the slope of the graph (**Figure 15**). The values of k_n and R^2 are shown in **Table 3**. The correlation coefficient R2 for the pseudo second order kinetic model is greater than 0.99.

3.4. Adsorption Isotherms

Adsorption data are generally described by adsorption isotherms, such as Freundlich, Langmuir, and Temkin isotherm models.

3.4.1. Freundlich Isotherm

This model proposes monolayer sorption with a heterogeneous energy distribution of active sites, accompanied by interactions between adsorbed molecules. The general form of this model is presented in the following equation [12] [32]:

$$q_e = K_F C_e 1/n \tag{12}$$

The linear form of the Equation (12) is [12] [33]:

$$\ln q_e = \ln K_F + 1/n \ln C_e \tag{12a}$$

This isotherm relates the amount of solute adsorbed at equilibrium per weight

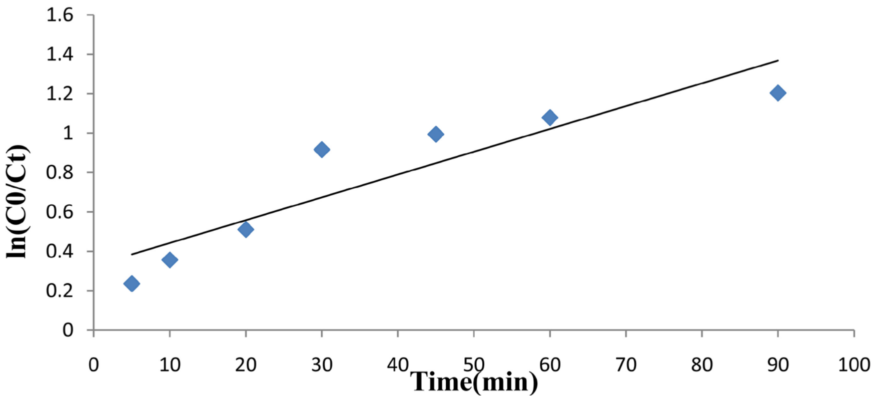

Figure 15. Natarajan and Khalaf plot for the adsorption of iron ions on HApMn.

of adsorbent where q_e (mol/g) to the adsorbate concentration at equilibrium C_e (mol/dm^3), is the most widely non-linear sorption models used. K_F (mg/g) stands for adsorption capacity and $1/n$ stands for adsorption intensity.

By plotting of $\ln q_e$ on Y-axis versus $\ln C$ on X-axis we can determine K_F and $1/n$ from a slope and intercept respectively (Figure 16).

3.4.2. Langmuir Isotherm

The Langmuir model [8] [26] [29] [32] describes adsorption as a monolayer surface corresponding to solids with identical homogeneous sites. This is according to the following linear relationship:

$$C_e / q_e = 1/\left(q_{\max} b\right) + \left(1/q_{\max}\right) C \tag{13}$$

where q_e is the amount adsorbed (mg/g), C_e is the equilibrium concentration of the adsorbate ions (mg/L), $q_{\max}$ and b are Langmuir constants. Where, $\mathrm{q}_{\max}$ (mg/g) is Langmuir constant related to maximum adsorption capacity (monolayer capacity) andb (L/mg) is the energy of adsorption.

By plotting of C_e/q_e versus C_e should indicate a straight line of slope $1/q_{\max}$ and an intercept of $1/q_{\max}\ b$.

Figure 17: shows Langmuir isotherm for iron ions adsorption at various initial iron ions concentrations using HApMn at adsorbent dosage of 0.1 g, agitation speed of 400 rpm, solution pH 6 and temperature of 30˚C. Based on the correlation coefficient (R^2) shown in Table 4 the adsorption isotherm can be better described by Langmuir equation. Also, the Langmuir equation yields a better fit of the experimental data than the Freundlich equation. Further, the essential characteristics of Langmuir isotherm can be described by a separation factor R_L, which indicates the shape of the isotherm and nature of the adsorption process. this is expressed by the following equation [8] [29] [30] [34].

$$R_L = \left[1/\ \left(1 + bC_o\right)\right] \tag{14}$$

where C_o is the initial concentration of iron ions (mg/L). The separation factor When R_L is greater than 1, the process is unfavourable, $R_L = 1$, Linear, $0 < R_L < 1$, favorable and $R_L = 0$ irreversible. In this study, the Calculated values for R_L are

Table 4. Adsorption isotherms constants.

Freundlich			Langmuir			Temkin		
K_f (mg/g)	1/*n*	R^2	q_{max} (mg/g)	*B* (L/mg)	R^2	*KT* (L/mg)	β (g/mg)	R^2
1.255	−0.222	0.799	0.603	−0.837	0.958	0.002	−0.201	−0.853

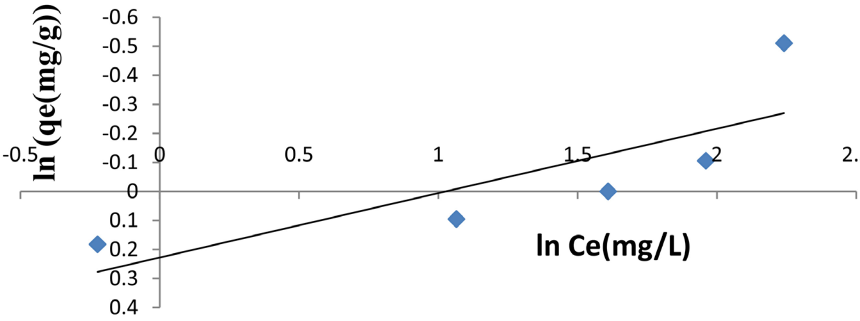

Figure 16. Freundlich isotherm for iron ions sorption on HApMn.

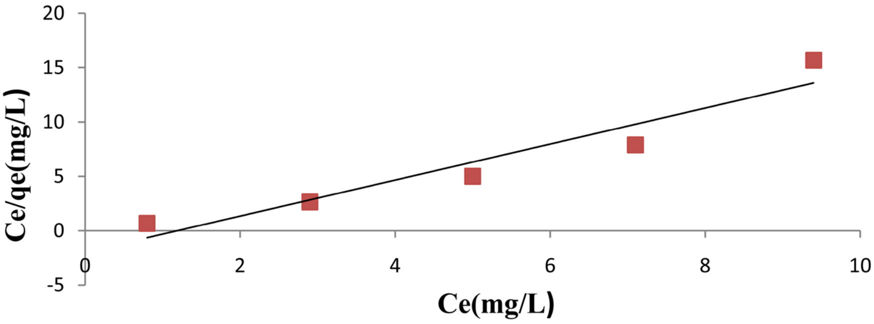

Figure 17. Langmuir isotherm for iron ions adsorption on HApMn.

found to be a fraction in the range of 0 - 1 (0.442), an indication that the adsorption process is favorable [35].

3.4.3. Temkin Isotherm

The linear form of the Temkin equation is given by [8] [29] [30] [36]:

$$q_e = \beta \ln KT + \beta \ln C_e \tag{15}$$

where, β which is related to the heat of adsorption, and *KT* (L/mg) is the equilibrium binding constant corresponding to the maximum binding energy. By plotting q_e on Y-axis versus on X-axis we can be calculated β and KT calculated from the slope and the intercept. **Figure 18**: shows Temkin model isotherm for iron ions adsorption at various initial iron ions concentrations using HApMn at adsorbent dosage of 0.1 g, agitation speed of 400 rpm, solution pH 6 and temperature of 25˚C.

3.5. Thermodynamic Parameters

Thermodynamic parameters [37] such as and entropy (ΔS), enthalpy (ΔH) and free energy (ΔG) were determined using Equations (16)-(19):

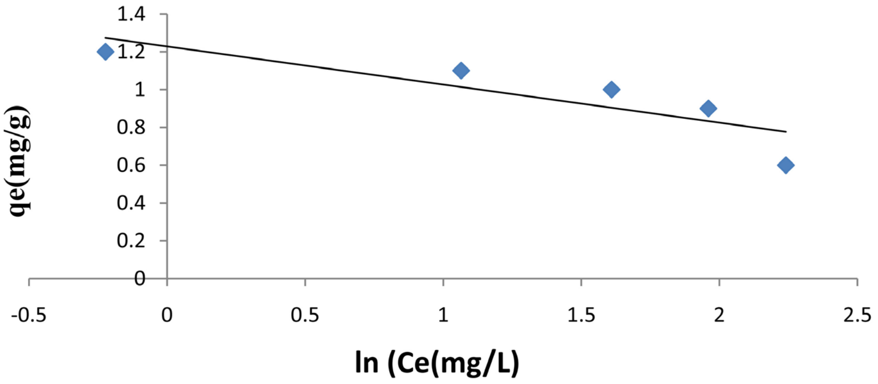

Figure 18. Temkin model plot for Adsorption of iron on HApMn.

$$K_c = q_e / C_e \tag{16}$$

$$\Delta G = -RT \ln K_c \tag{17}$$

$$\text{Ln}K_c = \left(-\Delta H/R\right)\left(1/T\right) + \Delta S/R \tag{18}$$

where q_e is the amount of solute adsorbed on the adsorbent cubic decimeter of the solution at equilibrium, K_c is the equilibrium constant, and C_e (mol/dm^3) is the equilibrium concentration of the solute in solution, T is temperature in Kelvin and R (8.314 J/K/mol) is the gas constant. By plotting of on Y-axis against $1/T$ on X-axis we found ΔH and ΔS were obtained from the slope and intercept of Vant Hoff isotherm (Figure 19). Table 5 shows the calculated values of the thermodynamic parameters.

In order to understand this process better, we must calculate the entropies and enthalpies of temperature periods using the previous equations [32] [38]:

$$\Delta G^{\circ} = \Delta H^{\circ} - T\Delta S^{\circ} \tag{19}$$

where, K_{c1} is the equilibrium constant at temperature T_1 and K_{c2} are the equilibrium constant at temperature T_2.

Increasing the value of ΔG° with increasing temperature leads to the process of adsorption of iron ions on HApMn become preferred in low temperatures. The negative value of ΔH° proves that the adsorption process was exothermic reaction and a certain amount of heat developed during the iron ions that adsorbed on the surface of the adsorbents. The more negative value of ΔS°, the more degree of randomization in the solid/liquid interface during the absorption process where entropy expresses the amount of randomness or disorder in the system.We used entropy (ΔS°) to determine the degree of disorder or randomness in the system. We know that the higher the negative values of ΔS°, the lower the degree of randomization in the solid/liquid interface during the adsorption process [39]. The values of ΔH° and ΔS° calculated from the plot of $\ln K$ versus $1/T$.

The value of ΔH° was negative, indicating that the adsorption reaction was exothermic (high heat of adsorption). Another equation that has been used to determine the possible adsorption mechanism is the **Dubinin-Radushkevick**

Table 5. Thermodynamic parameters for adsorption of iron ions on HApMn.

T (K)	K_c	ΔG (kg/mol)	ΔH	ΔS	R^2
298	1.5	0.405	−51	−142	0.991
318	0.379	−0.969			
333	0.200	−1.609			
348	0.127	−2.605			

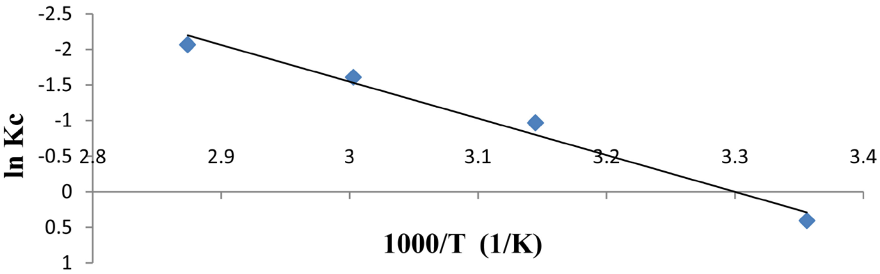

Figure 19. Thermodynamic model plot for Adsorption of iron ions on HApMn.

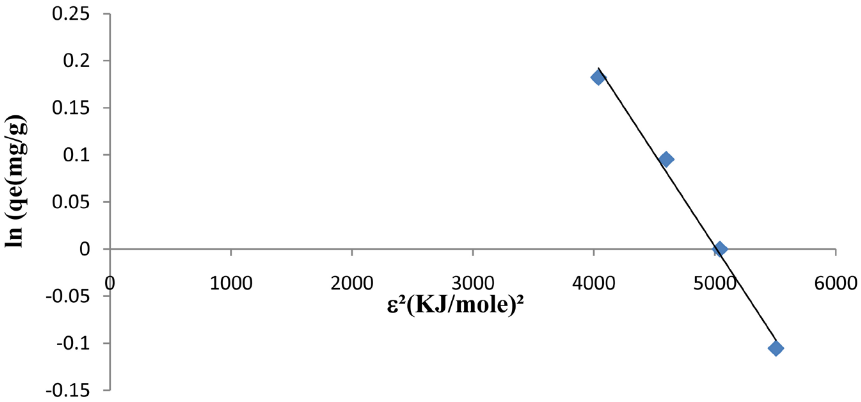

Figure 20. Dubinin-Radushkevick equation plot.

[40] equation, which assumes a constant sorption potential. The linear presentation of this equation is expressed by

$$\ln q_e = \ln q_m - K_E \varepsilon^2 \tag{20}$$

$$\varepsilon = RT \ln\left(1 + 1/C_e\right) \tag{21}$$

where ε is the Polanyi potential, q_t is the monolayer capacity (mol/g), C_e is the equilibrium concentration (mol/dm^3), and K_E is the constant related to sorption energy (mol^2/KJ^2) The parameters q_t and K_E can be obtained from the intercept and slope of the plot as shown in **Figure 20**. The free energy of sorption (E) is calculated by

$$E = 1/\left(-2K_E\right)^{1/2} \tag{22}$$

Adsorption type could be estimated by evaluating of E value. If this value is < 8, 8 - 16 or >16 kJ/mol, the adsorption type can be explained by physical adsorption, ion-exchange, or chemical adsorption, respectively [41]. In this case, the adsorption is chemical adsorption at all temperatures because E value was 50 kJ/mol.

4. Conclusion

In this article, we use Modified HApMn for removing iron ions from groundwater. Adsorption of iron on HApMn follows pseudo-second order kinetic model, Langmuir adsorption isotherm, Adsorption capacity from the Langmuir model is 0.604 mg/g, the adsorption process is chemical type because adsorption energy value is 50 kJ/mol, and adsorption is favorable at low temperatures, the negative value of ΔH° confirms that the sorption process is exothermic in nature and a given amount of heat is evolved during the binding iron ions on the surface of adsorbents.

Acknowlegements

It is my pleasure to express my deepest thanks to Chemistry Department, Faculty of Science, Helwan University, my thanks to Chemistry Department, Faculty of Science, Al-Azhar University, Assiut Branch, for his support and I thank Sohag Company for Water and Waste Water, Dar El Salam, Sohag, Egypt.

Conflicts of Interest

The authors declare no conflicts of interest regarding the publication of this paper.

References

[1] Hossain, D., Islam, M.S., Sultana, N. and Tusher, T.R. (2013) Assessment of Iron Contamination in Groundwater at Tangail Municipality, Bangladesh. *Journal of Environmental Science and Natural Resources*, **6**, 117-121. https://doi.org/10.3329/jesnr.v6i1.22051

[2] Prentice, A.M., *et al.* (2017) Dietary Strategies for Improving Iron Status: Balancing Safety and Efficacy. *Nutrition Reviews*, **75**, 49-60. https://doi.org/10.1093/nutrit/nuw055

[3] Abdennebi, N., Benhabib, K., Goutaudier, C. and Bagane, M. (2017) Removal of Aluminium and Iron Ions from Phosphoric Acid by Precipitation of Organo-Metallic Complex Using Organophosphorous Reagent. *Journal of Materials and Environmental Science*, **8**, 557-565.

[4] Dubey, S., Banerjee, S., Upadhyay, S.N. and Sharma, Y.C. (2017) Application of Common Nano-Materials for Removal of Selected Metallic Species from Water and Wastewaters: A Critical Review. *Journal of Molecular Liquids*, **240**, 656-677. https://doi.org/10.1016/j.molliq.2017.05.107

[5] Hosseini, H., Rezaei, H., Shahbazi, A. and Maghsudlu, A. (2016) Application of Nano-Lignocellulose for Removal of Nickel Ions from Aqueous Solutions. *Environmental Resource Research*, **4**, 213-229.

[6] Piuleac, C.G., Sáez, C., Cañizares, P. and Curteanu, S. (2012) Hybrid Model of a Wastewater-Treatment Electrolytic Process. *International Journal of Electrochemical Science*, **7**, 6289-6301.

[7] Mondal, P., Majumder, C.B. and Mohanty, B. (2008) Effects of Adsorbent Dose, Its Particle Size and Initial Arsenic Concentration on the Removal of Arsenic, Iron and Manganese from Simulated Ground Water by Fe3+ Impregnated Activated Carbon. *Journal of Hazardous Materials*, **150**, 695-702. https://doi.org/10.1016/j.jhazmat.2007.05.040

[8] Javadian, H., Ghorbani, F., Tayebi, H. and Asl, S.H. (2015) Study of the Adsorption of Cd (II) from Aqueous Solution Using Zeolite-Based Geopolymer, Synthesized from Coal Fly Ash; Kinetic, Isotherm and Thermodynamic Studies. *Arabian Journal of Chemistry*, **8**, 837-849. https://doi.org/10.1016/j.arabjc.2013.02.018

[9] Agarwal, S., *et al.* (2016) Efficient Removal of Toxic Bromothymol Blue and Methylene Blue from Wastewater by Polyvinyl Alcohol. *Journal of Molecular Liquids*, **218**, 191-197. https://doi.org/10.1016/j.molliq.2016.02.060

[10] Bhatnagar, A. and Sillanpää, M. (2017) Removal of Natural Organic Matter (NOM) and Its Constituents from Water by Adsorption—A Review. *Chemosphere*, **166**, 497-510. https://doi.org/10.1016/j.chemosphere.2016.09.098

[11] Mrinal, D.D., Adak, K., Mondal, B., Dhak, P. and Sen, S. (2017) A Comparative Study on Fluoride Removal Capacity from Drinking Water by Adsorption Using Nano-Sized Alumina and Zirconia Modified Alumina Prepared by Chemical Route. *Advances in Water Science and Technology*, **4**, 1-10.

[12] Abuh, M.A., Akpomie, G.K., Nwagbara, N.K., Abia-Bassey, N., Ape, D.I. and Ayabie, B.U. (2013) Kinetic Rate Equations Application on the Removal of Copper (II) and Zinc (II) by Unmodified Lignocellulosic Fibrous Layer of Palm Tree Trunk-Single Component System Studies. *International Journal of Basic and Applied Sciences*, **50**, 800-809.

[13] Elhafez, S.E.A., Hamad, H.A., Zaatout, A.A. and Malash, G.F. (2017) Management of Agricultural Waste for Removal of Heavy Metals from Aqueous Solution: Adsorption Behaviors, Adsorption Mechanisms, Environmental Protection, and Techno-Economic Analysis. *Environmental Science and Pollution Research*, **24**, 1397-1415. https://doi.org/10.1007/s11356-016-7891-7

[14] Voisin, H., Bergström, L., Liu, P. and Mathew, A. (2017) Nanocellulose-Based Materials for Water Purification. *Nanomaterials*, **7**, 57. https://doi.org/10.3390/nano7030057

[15] Bhadra, B.N., Ahmed, I., Kim, S. and Jhung, S.H. (2017) Adsorptive Removal of Ibuprofen and Diclofenac from Water Using Metal-Organic Framework-Derived Porous Carbon. *Chemical Engineering Journal*, **314**, 50-58. https://doi.org/10.1016/j.cej.2016.12.127

[16] Wang, X., Liang, Y., An, W., Hu, J., Zhu, Y. and Cui, W. (2017) Removal of Chromium (VI) by a Self-Regenerating and Metal Free g-C_3N_4/Graphene Hydrogel System via the Synergy of Adsorption and Photo-Catalysis under Visible Light. *Applied Catalysis B: Environmental*, **219**, 53-62. https://doi.org/10.1016/j.apcatb.2017.07.008

[17] Sarker, M., Bhadra, B.N., Seo, P.W. and Jhung, S.H. (2017) Adsorption of Benzotriazole and Benzimidazole from Water over a Co-Based Metal Azolate Framework MAF-5(Co). *Journal of Hazardous Materials*, **324**, 131-138. https://doi.org/10.1016/j.jhazmat.2016.10.042

[18] Elkady, M.F., Mahmoud, M.M. and Abd-El-Rahman, H.M. (2011) Kinetic Approach for Cadmium Sorption Using Microwave Synthesized Nano-Hydroxyapatite. *Journal of Non-Crystalline Solids*, **357**, 1118-1129. https://doi.org/10.1016/j.jnoncrysol.2010.10.021

[19] Gotić, M., Jurkin, T., Musić, S., Unfried, K., Sydlik, U. and Bauer-Šegvić, A. (2013) Microstructural Characterizations of Different Mn-Oxide Nanoparticles Used as Models in Toxicity Studies. *Journal of Molecular Structure*, **1044**, 248-254. https://doi.org/10.1016/j.molstruc.2012.09.083

[20] Abdel Ghafar, H.H., Ali, G.A.M., Fouad, O.A. and Makhlouf, S.A. (2015) Enhancement of Adsorption Efficiency of Methylene Blue on Co3O4/SiO2 Nanocomposite. *Desalination and Water Treatment*, **53**, 2980-2989. https://doi.org/10.1080/19443994.2013.871343

[21] Hamdaoui, O. (2017) Adsorption of Cu(II) from Aqueous Phase by Cedar Bark. *Journal of Dispersion Science and Technology*, **38**, 1087-1091. https://doi.org/10.1080/01932691.2016.1225261

[22] Gupta, V.K., Agarwal, S., Sadegh, H., Ali, G.A.M., Bharti, A.K. and Hamdy Makhlouf, A.S. (2017) Facile Route Synthesis of Novel Graphene Oxide-*β*-Cyclodextrin Nanocomposite and Its Application as Adsorbent for Removal of Toxic Bisphenol A from the Aqueous Phase. *Journal of Molecular Liquids*, **237**, 466-472. https://doi.org/10.1016/j.molliq.2017.04.113

[23] Gomaa, H., Gomaa, A., Farid, M., Cheira, M., Ahmed, T. and Seaf, S.E.T.A. (2016) Removal of Uranium from Acidic Solution Using Activated Carbon Impregnated with Tri Butyl Phosphate. *Biological and Chemical Research*, 313-340.

[24] Gomaa, H., *et al.* (2018) Highly-Efficient Removal of AsV, $Pb^{2+,}$ $Fe^{3+,}$ and Al^{3+} Pollutants from Water Using Hierarchical, Microscopic TiO_2 and $TiOF_2$ Adsorbents through Batch and Fixed-Bed Columnar Techniques. *Journal of Cleaner Production*, **182**, 910-925. https://doi.org/10.1016/j.jclepro.2018.02.063

[25] Abd El-Latif, M.M. and Elkady, M.F. (2011) Kinetics Study and Thermodynamic Behavior for Removing Cesium, Cobalt and Nickel Ions from Aqueous Solution Using Nano-Zirconium Vanadate Ion Exchanger. *Desalination*, **271**, 41-54. https://doi.org/10.1016/j.desal.2010.12.004

[26] Elnasr, A.T.S., Soliman, M.H. and Ayash, M.A.-E.-A.A. (2017) Modified Hydroxyapatite Adsorbent for Removal of Iron Dissolved in Water Wells in Sohag, Egypt. *Chemistry of Advanced Materials*, **1**, 1-13.

[27] Habeeb, O.A., *et al.* (2016) Modeling and Optimization for H2S Adsorption from Wastewater Using Coconut Shell Based Activated Carbon. *Australian Journal of Basic and Applied Sciences*, **10**, 136-147.

[28] Shah, A.F.S., Ajit, M.S. and Usmani, G.A. (2016) Kinetics Modelling Study: Adsorption of Victoria Blue on Mahaneem Leaf Powder. *International Journal of Advanced Scientific and technical Research*, **1**, 293-302.

[29] Habeeb, O.A., *et al.* (2016) Modeling and Optimization for H2S Adsorption from Wastewater Using Coconut Shell Based Activated Carbon. *Australian Journal of Basic and Applied Sciences*, **10**, 136-147.

[30] Dehghani, M.H., Sanaei, D., Ali, I. and Bhatnagar, A. (2016) Removal of Chromium (VI) from Aqueous Solution Using Treated Waste Newspaper as a Low-Cost Adsorbent: Kinetic Modeling and Isotherm Studies. *Journal of Molecular Liquids*, **215**, 671-679. https://doi.org/10.1016/j.molliq.2015.12.057

[31] Ioannou, Z. and Simitzis, J. (2009) Adsorption Kinetics of Phenol and 3-Nitrophenol from Aqueous Solutions on Conventional and Novel Carbons. *Journal of Hazardous Materials*, **171**, 954-964. https://doi.org/10.1016/j.jhazmat.2009.06.098

[32] Romero-González, J., Peralta-Videa, J.R., Rodriíguez, E., Ramirez, S.L. and Gardea-Torresdey, J.L. (2005) Determination of Thermodynamic Parameters of Cr(VI) Adsorption from Aqueous Solution onto *Agave lechuguilla* Biomass. *The Journal of*

Chemical Thermodynamics, **37**, 343-347. https://doi.org/10.1016/j.jct.2004.09.013

[33] Zamani, S., Salahi, E. and Mobasherpour, I. (2013) Removal of Nickel from Aqueous Solution by Nano Hydroxyapatite Originated from Persian Gulf Corals. *Canadian Chemical Transactions*, **1**, 173-190. https://doi.org/10.13179/canchemtrans.2013.01.03.0033

[34] Demirkıran, N., Özdemir, G.D.T., Saraç, M. and Dardağan, M. (2017) Adsorption of Methylene Blue from Aqueous Solutions by Pyrolusite Ore. *Mongolian Journal of Chemistry*, **18**, 5-11. https://doi.org/10.5564/mjc.v18i44.880

[35] Kooh, M.R.R., Lim, L.B.L., Lim, L.H. and Dahri, M.K. (2016) Separation of Toxic Rhodamine B from Aqueous Solution Using an Efficient Low-Cost Material, *Azolla pinnata*, by Adsorption Method. *Environmental Monitoring and Assessment*, **188**, 1-15. https://doi.org/10.1007/s10661-016-5108-7

[36] Wang, W. and Wang, J. (2018) Comparative Evaluation of Sorption Kinetics and Isotherms of Pyrene onto Microplastics. *Chemosphere*, **193**, 567-573. https://doi.org/10.1016/j.chemosphere.2017.11.078

[37] Foroutan, R., Esmaeili, H., Abbasi, M., Rezakazemi, M. and Mesbah, M. (2018) Adsorption Behavior of Cu(II) and Co(II) Using Chemically Modified Marine Algae. *Environmental Technology*, **39**, 2792-2800. https://doi.org/10.1080/09593330.2017.1365946

[38] Lima, E.C., Hosseini-Bandegharaei, A., Moreno-Piraján, J.C. and Anastopoulos, I. (2019) A Critical Review of the Estimation of the Thermodynamic Parameters on Adsorption Equilibria. Wrong Use of Equilibrium Constant in the Van't Hoof Equation for Calculation of Thermodynamic Parameters of Adsorption. *Journal of Molecular Liquids*, **273**, 425-434. https://doi.org/10.1016/j.molliq.2018.10.048

[39] Labib, S.A., Yousif, A.M., Ibrahim, I.A. and Atia, A.A. (2018) Adsorption of Rhodium by Modified Mesoporous Cellulose/Silica Sorbents: Equilibrium, Kinetic, and Thermodynamic Studies. *Journal of Porous Materials*, **25**, 383-396. https://doi.org/10.1007/s10934-017-0449-3

[40] Kamga, F.T. (2019) Modeling Adsorption Mechanism of Paraquat onto Ayous (*Triplochiton scleroxylon*) Wood Sawdust. *Applied Water Science*, **9**, 1. https://doi.org/10.1007/s13201-018-0879-3

[41] Khatibikamal, V., Panahi, H.A., Torabian, A. and Baghdadi, M. (2019) Optimized Poly(amidoamine) Coated Magnetic Nanoparticles as Adsorbent for the Removal of Nonylphenol from Water. *Microchemical Journal*, **145**, 508-516. https://doi.org/10.1016/j.microc.2018.11.018